Raideur en cisaillement transverse du module à chevrons utilisé comme âme de panneaux sandwich = Transverse Shear Stiffness of a Chevron Folded Core Used in Sandwich Construction

Arthur Lebée, Karam Sab

Raideur en cisaillement transverse du module à chevrons utilisé comme âme de panneaux sandwich

Transverse Shear Stiffness of a Chevron Folded Core Used in Sandwich Construction

A. Lebée [1], K. Sab [1]

1: UR Navier - Université Paris-Est. École des Ponts Paris Tech,
6 et 8 avenue Blaise Pascal.
77455 Marne-la-Vallée cedex2
e-mail: sab@lami.enpc.fr, arthur.lebee@lami.enpc.fr

Résumé

En se basant sur la méthode proposée par Kelsey et al. [1], les bornes supérieures et inférieures de la raideur en cisaillement transverse d'une âme pliée en module à chevrons sont déterminées analytiquement et comparées au calcul par éléments finis. On observe que ces bornes sont généralement assez larges et qu'il existe des configurations géométriques pour lesquelles le module à chevrons peut être jusqu'à 40% plus raide que les nids d'abeille.

Abstract

Using Kelsey et al. [1] unit load method, upper and lower bounds for transverse shear stiffness of a chevron folded core used in sandwich construction are analytically derived and compared to finite element computations. It is found that these bounds are generally loose and that some chevron folded cores are 40% stiffer than honycomb cores.

Mots Clés: panneaux sandwich, âme pliées, module de cisaillement, module à chevrons
Keywords: Sandwich panels, Folded cores, Shear modulus, Chevron pattern

1. Introduction

Sandwich panels made of two thin skins separated by a thick periodic core are commonly used in many fields. They offer good compromise between strength and weight especially for aeronautics applications.

When bending the sandwich panel, the skins are subjected to in-plane traction and compression whereas the core is subjected to transverse shear. Many constituents can be used as core materials. Balsa glued between stiffer pieces of wood was one of the first attempts to make a sandwich panel. Nowadays, phenolic paper honeycomb is extensively used in aeronautics structures.

Recently, new types of promising cores have emerged. Folded cores are promising because of new production means [2, 3, 4, 5]. Among them, chevron folded core was probably the first to be machined (Fig. 1).

It seems that Chevron folded cores manufacturing was first considered at the beginning of the 20^{th} century. Later, the pattern has been under investigation in Kazan University. More recently, continuous production and several new techniques emerged [6, 7, 8, 9]. Chevron folded cores strength has been experimentally investigated in [2, 5, 3] and simulated in [3, 4, 10]. Their transverse shear stiffness is also under investigation in [5] but to the authors knowledge it seems that no theoretical work has been done yet.

The aim of this paper is to derive bounds for the transverse shear stiffness of chevron folded cores. Kelsey *et al.* [1] proposed a method for deriving such bounds for honeycomb cores. One may refer also to [11] for a detailed description of this method. Many honeycomb geometries have already been assessed [12, 13], new homogenization methods have been proposed [14],[15], and more attention has been paid to the skin effect on the effective transverse shear stiffness of the core material [16]. However, as a first attempt for the determination of the transverse shear stiffness of folded chevron, it seems relevant to use Kelsey *et al.*[1] method.

According to this method, the minimum potential energy theorem is used for deriving upper bounds for the transverse shear modulus in the $\alpha-$direction, $G_{\alpha 3}$. A uniform horizontal displacement $h\gamma_{\alpha 3}$ in the $\alpha-$direction is imposed to the top face of the core material while its lower face is fixed (Fig. 2). Here, $\alpha = 1, 2$ are the in-plane directions, $\gamma_{\alpha 3}$ is the transverse shear strain in the $\alpha-$direction and h is the height of the core. Then, the normalized strain energy of any trial strain field which is piecewise uniform in the core walls and compatible with the kinematic boundary conditions provides an upper bound for $G_{\alpha 3}$, noted $G^{+}_{\alpha 3}$. Similarly,

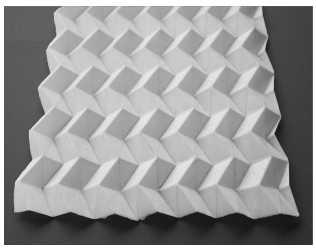

Fig. 1. Chevron folded paper.

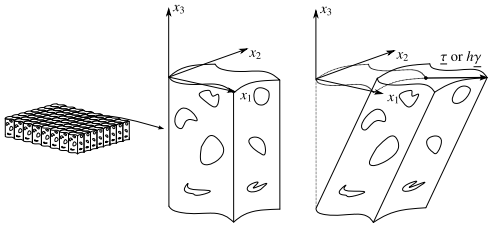

Fig. 2. Kelsey et al. unit load method

the minimum complementary energy theorem is used for deriving lower bounds for $G_{\alpha 3}$. A uniform horizontal stress load $\tau_{\alpha 3}$ (respectively, $-\tau_{\alpha 3}$) is applied in the $\alpha-$direction to the upper (respectively, lower) face of the core material. Then, the normalized stress energy of any piecewise uniform trial stress field which is statically compatible with the boundary conditions provides a lower bound for $G_{\alpha 3}$, noted $G^{-}_{\alpha 3}$.

2. The chevron pattern

Like honeycomb, the chevron pattern is periodic in the in-plane directions. Four identical parallelogram - shape faces are necessary to generate the whole pattern by periodicity along the $\underline{e}_1$ vector (period $2a$) and the $\underline{e}_2$ vector (period $2s$) where $\mathcal{M} = (A, \underline{e}_1, \underline{e}_2, \underline{e}_3)$ is the main coordinate system. Fig. 3 shows these faces: face 1= $ABCD$, face 2= $D'CBA'$, face 3= $\overline{A'''B'''CD'}$ and face 4 = $DCB''A''$.

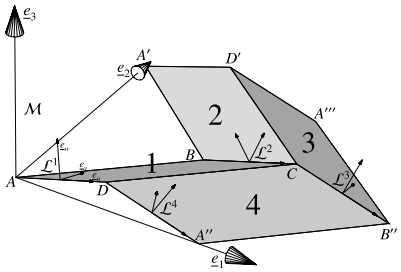

Fig. 3. The four elementary faces of the pattern.

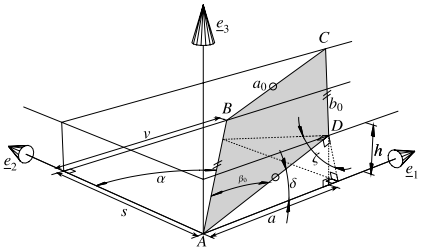

Fig. 4. Face 1.

Tab. 1 gives vertices coordinates in terms of four geometric parameters: a, s, v and h where v is a horizontal offset parameter ($v = 0$ when B is aligned with A and A') and h is the pattern height.

Point	A	B	C	D	A'	D'	A''	B''	A'''
x_1	0	v	$a+v$	a	0	a	$2a$	$2a+v$	$2a$
x_2	0	s	s	0	$2s$	$2s$	0	s	$2s$
x_3	0	0	h	h	0	h	0	0	0

Tab. 1. Vertices coordinates.

Actually, several parameters sets have been proposed for the geometric description of the chevron pattern [8, 17]. Among them, the set a_0, b_0, δ, ζ fully determines the geometry and the position of face 1. Face 1 is a parallelogram (a_0 and b_0 are the side lengths) which is tilted by angles δ and ζ with respect to the main coordinate system as shown in Fig. 4.

- δ is the *member angle* by analogy with truss beams: cutting the chevron pattern by the $(A, \underline{e}_1, \underline{e}_3)$ plane gives a zigzag shape similar to that of a Warren-type truss beam.
- ζ is the *closure angle* equal to the half angle between face 1 and face 2 along the BC edge. For $\zeta = 0$ the pattern is completely folded and for $\zeta = \pi/2$ the pattern is prismatic.
- $\beta_0 = \arctan \frac{\tan \delta}{\cos \zeta}$ is the $\widehat{DAB}$ angle and $\alpha = \arctan \frac{1}{\tan \zeta \sin \delta}$ is the $\widehat{A'AB}$ angle

We have: $a = a_0 \cos \delta$, $s = b_0 \cos \alpha$, $v = b_0 \sin \alpha$, $h = a_0 \sin \delta$. Fig. 5 shows the pattern aspect of the unit cell for several values of ζ and δ ($a_0/b_0 = 1$).

The chevron pattern has actually three major symmetries. When used as a core between two isotropic skins, these symmetries lead to several simplifications in the Reissner-Mindlin plate constitutive law [18]. Fig. 6

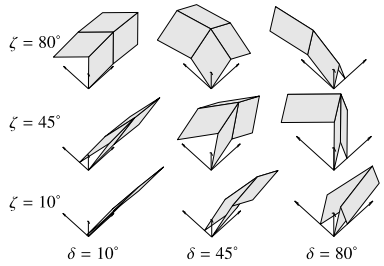

Fig. 5. Several configurations ($a_0/b_0 = 1$).

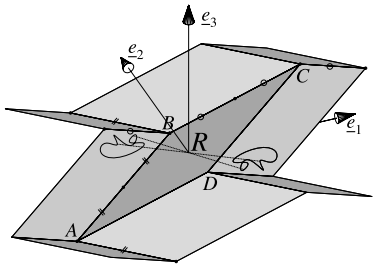

Fig. 6. Central symmetry with respect to point R.

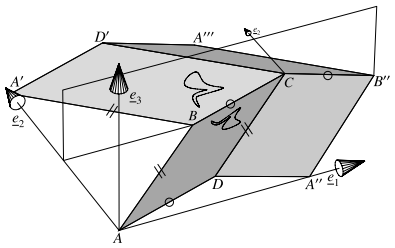

Fig. 7. Symmetry with respect to $(B, \underline{e}_1, \underline{e}_3)$ plane.

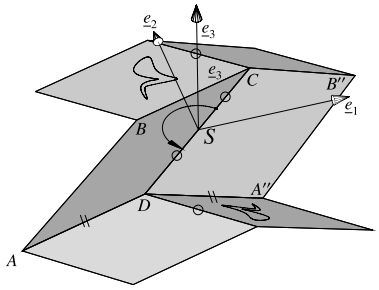

Fig. 8. Rotational symmetry with respect to $(S, \underline{e}_3)$ axis.

shows the central symmetry $\mathcal{R}$ with respect to the center point of face 1, R. This symmetry uncouples in-plane (membrane) stress and out-of-plane (flexural) stress. Fig. 7 shows the symmetry $\mathcal{N}$ with respect to the $(B, \underline{e}_1, \underline{e}_3)$ plane. This symmetry uncouples transverse shear stresses. Fig. 8 shows the rotational symmetry $\mathcal{S}$ of axis $(S, \underline{e}_3)$. This symmetry uncouples transverse shear stress and tensile stress in direction 3. Finally, there are only two transverse shear moduli to be determined: G_{13} and G_{23}.

It is useful to introduce a local basis $\mathcal{L}^k = (\underline{e}^k_u, \underline{e}^k_v, \underline{e}^k_w)$ associated to face k ($k = 1, 2, 3, 4$) as shown in Fig. 3. For face 1, vector $\underline{e}^1_u$ is along the AD edge, $\underline{e}^1_w$ is normal to the face with $\underline{e}^1_w \cdot \underline{e}_3 > 0$ and $\underline{e}^1_v$ is such that $\mathcal{L}^1$ is direct. Thus, the components of $(\underline{e}^1_u, \underline{e}^1_v, \underline{e}^1_w)$ in the $(\underline{e}_1, \underline{e}_2, \underline{e}_3)$ basis are given by:

$$(\underline{e}^1_u, \underline{e}^1_v, \underline{e}^1_w) = \begin{pmatrix} \cos\delta & \sin\zeta\cos\delta & -\sin\delta\sin\zeta \\ 0 & \sin\zeta & \cos\zeta \\ \sin\delta & -\cos\delta\cos\zeta & \cos\delta\sin\zeta \end{pmatrix}_{(\underline{e}_1,\underline{e}_2,\underline{e}_3)} \qquad \text{(eq. 1)}$$

Moreover, the symmetries enables to determine the components of the other local basis $\mathcal{L}^2$, $\mathcal{L}^3$ and $\mathcal{L}^4$.

3. Analytical bounds

3.1 Lower bounds

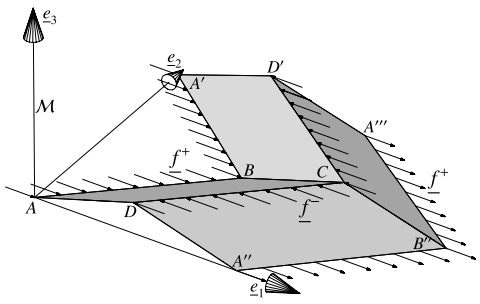

Fig. 9. Stress load in direction 1.

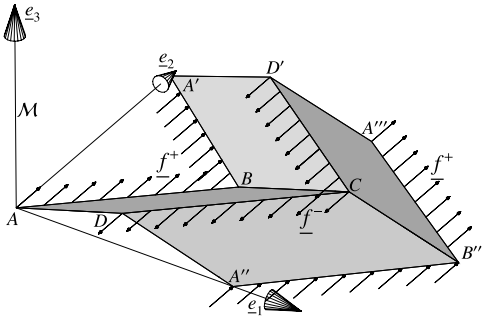

Fig. 10. Stress load in direction 2.

According to Kelsey *et al.*[1] method, a uniformly distributed horizontal force per unit length, $\underline{f}^{\pm}$, is applied to the upper (+) and lower edges ($-$) of the pattern as shown in Fig. 9 and 10:

$$\underline{f}^{\pm} = \pm 2 \frac{a\,s}{b_0} \tau_\alpha \underline{e}_\alpha \qquad \text{(eq. 2)}$$

Piecewise uniform plane stress is assumed in each face. Hence, the stress of face 1 writes:

$$\underline{\underline{\sigma}}^1 = \sigma^1_{uu} \underline{e}^1_u \otimes \underline{e}^1_u + \sigma^1_{vv} \underline{e}^1_v \otimes \underline{e}^1_v + \sigma^1_{uv} \left(\underline{e}^1_u \otimes \underline{e}^1_v + \underline{e}^1_v \otimes \underline{e}^1_u \right) \qquad \text{(eq. 3)}$$

where $\otimes$ is the dyadic product of two vectors and σ^1_{uu} , σ^1_{vv}, σ^1_{uv} are three unknowns to be determined. Thanks to $\mathcal{N}$ and $\mathcal{S}$ symmetries, it is possible to express the stress $\underline{\underline{\sigma}}^k$ of face k , $k = 2, 3, 4$, in terms of $\underline{\underline{\sigma}}^1$. Indeed, the following relations are easily derived:

$$\underline{\underline{\sigma}}^2 = \epsilon \underline{\underline{\mathcal{N}}}\, \underline{\underline{\sigma}}^1 \underline{\underline{\mathcal{N}}}, \quad \underline{\underline{\sigma}}^4 = -\underline{\underline{\mathcal{S}}}\, \underline{\underline{\sigma}}^1 \underline{\underline{\mathcal{S}}}, \quad \underline{\underline{\sigma}}^3 = \epsilon \underline{\underline{\mathcal{N}}}\, \underline{\underline{\sigma}}^4 \underline{\underline{\mathcal{N}}}, \qquad \text{(eq. 4)}$$

where $\epsilon = 1$ for loading in direction 1 and $\epsilon = -1$ for loading in direction 2. The equilibrium condition at edge *AD* (or edge *BC*) writes :

$$\underline{\underline{\sigma}}^1 \cdot \underline{e}^1_v + \underline{\underline{\sigma}}^2 \cdot \left(-\underline{e}^2_v \right) = \underline{0} \qquad \text{(eq. 5)}$$

Similarly, the equilibrium condition at edge *CD* (or edge *AB*) writes:

$$-t \left(\underline{\underline{\sigma}}^1 \cdot \underline{n}^1 + \underline{\underline{\sigma}}^4 \cdot \underline{n}^4 \right) + \underline{f}^+ = 0 \qquad \text{(eq. 6)}$$

where t is the faces thickness and $\underline{n}^k$ is the in-plane vector of face k, $k = 1, 4$, which is outer normal to *CD*:

$$\underline{n}^1 = -\sin\beta_0 \underline{e}^1_u + \cos\beta_0 \underline{e}^1_v \qquad \underline{n}^4 = \sin\beta_0 \underline{e}^4_u - \cos\beta_0 \underline{e}^4_v \qquad \text{(eq. 7)}$$

The six (non independent) linear equations (eq. 5 - eq. 6) uniquely determine the three unknowns σ^1_{uu}, σ^1_{vv}, σ^1_{uv}. The solution is:

loading in direction 1:	loading in direction 2:
$\sigma^1_{uu} = -\sin\zeta \frac{a_0 \tau_1}{t}$	$\sigma^1_{uu} = -\cos\zeta \cos\delta \left(\frac{1}{\tan\delta} - \tan\delta \right) \frac{a_0 \tau_2}{t}$
$\sigma^1_{vv} = 0$	$\sigma^1_{vv} = 0$
$\sigma^1_{uv} = 0$	$\sigma^1_{uv} = -\cos\delta \frac{a_0 \tau_2}{t}$

The faces constitutive material is assumed to be isotropic[1]. Hence, the total stress energy of the unit cell is given by:

$$W^*_{int} = 2 \sin\beta_0 b_0 a_0 t \left(\frac{2(1+\nu_s)}{E_s} (\sigma^1_{uv})^2 + \frac{1}{E_s} (\sigma^1_{uu})^2 \right) \qquad \text{(eq. 8)}$$

where E_s and ν_s are the solid Young modulus and Poisson's ratio. The stress energy of the effective core material subjected to the transverse shear stress τ_α in the direction α is:

$$W^*_{ext} = 2ahs \frac{\tau_\alpha^2}{G_{\alpha 3}} \qquad \text{(eq. 9)}$$

The theorem of the complementary energy states that $W^*_{ext} \leq W^*_{int}$. Inserting the expressions of σ^1_{uu} and σ^1_{uv} into (eq. 8) gives the lower bounds:

$$G_{13} \geq G^-_{13} = \frac{t}{a_0} E_s \, \frac{\sin\delta \cos\delta}{\sin\zeta}$$
$$G_{23} \geq G^-_{23} = \frac{t}{a_0} E_s \, \frac{\sin\delta}{\cos\delta} \, \frac{\sin\zeta}{2(1+\nu_s) + \cos^2\zeta \left(\frac{1}{\tan\delta} - \tan\delta \right)^2}$$

It is more convenient to use the following normalization: $\mathcal{E}_\alpha = \frac{G_{\alpha 3}}{\rho G_s}$, where ρ is the core relative density, G_s is the solid shear modulus and $\mathcal{E}_\alpha$ is the normalized transverse shear modulus in direction α. For chevron cores, ρ is given by:

$$\rho = \frac{t}{a_0 \sin\zeta \sin\delta \cos\delta} \qquad \text{(eq. 10)}$$

[1] This is the case for metallic cores and for Nomex paper core. For CFRP cores, anisotropy should be introduced.

Hence, we have:

$$\mathcal{E}_1 \geq \mathcal{E}_1^- = 2(1+\nu_s)\ \sin^2\delta\cos^2\delta$$
$$\mathcal{E}_2 \geq \mathcal{E}_2^- = 2(1+\nu_s)\ \frac{\sin^2\delta\sin^2\zeta}{2(1+\nu_s)+\cos^2\zeta\left(\frac{1}{\tan\delta}-\tan\delta\right)^2}$$

3.2 Upper bounds

In order to derive an upper bound for the transverse shear modulus $G_{\alpha 3}$, a relative horizontal displacement, $\gamma_\alpha h$, between the top and the bottom of the chevron pattern is prescribed in the direction α as shown in Fig. 11 and 12. The corresponding overall transformation is:

$$\underline{\underline{F}} = \underline{\underline{I}} + \gamma_\alpha \underline{e}_\alpha \otimes \underline{e}_3 \qquad \text{(eq. 11)}$$

where $\underline{\underline{I}}$ is the unit second order tensor.

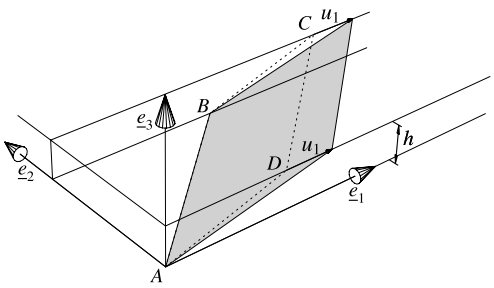

Fig. 11. Face 1 displacement in direction 1.

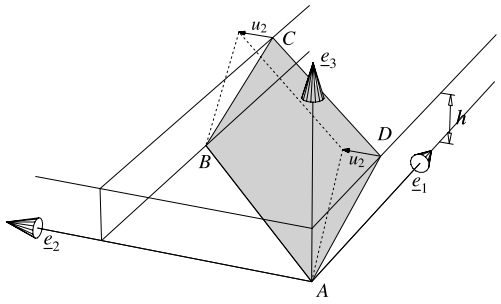

Fig. 12. Face 1 displacement in direction 2.

The in-plane components of the uniform Green-Lagrange strain tensor of face 1 with respect to the $(\underline{e}^1_u, \underline{e}^1_v)$ local basis are given by:

$$e^1_{\lambda\mu} = \frac{1}{2}\left(\underline{e}^{1*}_\lambda \cdot \underline{e}^{1*}_\mu - \delta_{\lambda\mu}\right) \qquad \lambda,\mu = u,v, \qquad \text{(eq. 12)}$$

where $\underline{e}^{1*}_\lambda = \underline{\underline{F}} \cdot \underline{e}^1_\lambda$, and $\delta_{\lambda\mu}$ is the Krönecker symbol. Neglecting the second order terms in γ_α leads to the following linearized in-plane strain components:

loading in direction 1	loading in direction 2
$\varepsilon^1_{uu} = \gamma_1 \sin\delta\cos\delta$	$\varepsilon^1_{uu} = 0$
$\varepsilon^1_{vv} = -\gamma_1 \sin\delta\cos\delta\cos^2\zeta$	$\varepsilon^1_{vv} = -\gamma_2\cos\zeta\sin\zeta\cos\delta$
$\varepsilon^1_{uv} = -\frac{\gamma_1}{2}\cos 2\delta\cos\zeta$	$\varepsilon^1_{uv} = \frac{\gamma_2}{2}\sin\zeta\sin\delta$

Piecewise uniform plane stress is assumed in each face. Therefore, the strain energy density of face 1 is given by:

$$w = \frac{1}{2}\left(\frac{E_s}{1+\nu_s}\left((\varepsilon^1_{uu})^2 + (\varepsilon^1_{vv})^2 + 2(\varepsilon^1_{uv})^2\right) + \frac{\nu_s E_s}{1-\nu_s^2}\left(\varepsilon^1_{uu}+\varepsilon^1_{vv}\right)^2\right). \qquad \text{(eq. 13)}$$

The total strain energy stored in the unit cell is:

$$W_{int} = 2\sin\beta_0 b_0 a_0 t w. \qquad \text{(eq. 14)}$$

The strain energy stored in the effective core material is:

$$W_{ext} = 2ahsG_{\alpha 3}\gamma_\alpha^2 \qquad \text{(eq. 15)}$$

According to the potential energy theorem, we have $W_{ext} \leq W_{int}$. Hence, the following upper bounds for the normalized transverse shear moduli are obtained:

$$\mathcal{E}_1 \leq \mathcal{E}_1^+ = \frac{2}{1-\nu_s}\sin^2\delta\cos^2\delta\sin^4\zeta + \cos^2\zeta$$
$$\mathcal{E}_2 \leq \mathcal{E}_2^+ = \sin^2\zeta\left(\frac{2}{1-\nu_s}\cos^2\delta\cos^2\zeta + \sin^2\delta\right)$$

3.3 Results

As expected, for both directions, we have: $0 < \mathcal{E}_\alpha^- \leq \mathcal{E}_\alpha^+ < 1$, where $\mathcal{E} = 1$ is associated to the Voigt upper bound and $\mathcal{E} = 0$ is associated to the Reuss lower bound. It should be emphasized that the derived bounds are only functions of ν_s and the angles ζ and δ.

Fig. 13 and 14 show the normalized lower and upper bounds in direction 1 as functions of δ and ζ for $\nu_s = 0.4$. It is possible to give a simple interpretation for the lower bound $\mathcal{E}_1^-$. The corresponding trial stress has only one non-zero component: σ_{uu}. All the faces are subjected to uniaxial traction and compression in the $\underline{e}_u$ direction. This structural behavior can be compared to Warren truss beams where members are under alternative traction and compression. Hence, it is not surprising that the lower bound depends only on the member angle δ and is maximum for $\delta = \pi/4$ as for Warren truss beams. For most values of ζ and δ, $\mathcal{E}_1^-$ and $\mathcal{E}_1^+$ are not equal. However, for $\delta = \pi/4$ and $\cos^2\zeta = \nu_s$, they are coincident ($\mathcal{E}_1^- = \mathcal{E}_1^+ = \frac{1+\nu_s}{2}$). This means that, for this geometric configuration, the piecewise uniform trial strain and stress fields are the exact solutions for the transverse shear loading in direction 1.

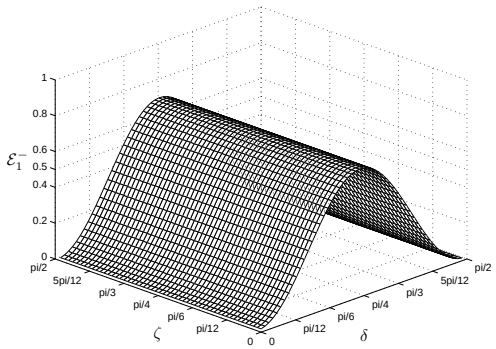

Fig. 13. $\mathcal{E}_1^-$ as function of ζ and δ for $\nu_s = 0.4$.

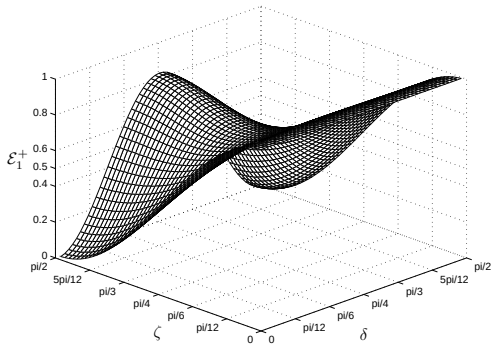

Fig. 14. $\mathcal{E}_1^+$ as function of ζ and δ for $\nu_s = 0.4$.

Fig. 15 and 16 show the normalized lower and upper bounds in direction 2. The trial stress field associated to $\mathcal{E}_2^-$ is mainly in-plane shear of the core walls as it is the case for a honeycomb core. For $\zeta = \pi/2$, the pattern is prismatic and both bounds are equal to $\sin^2\delta$ which is an exact value for $\mathcal{E}_2$. Actually, prismatic

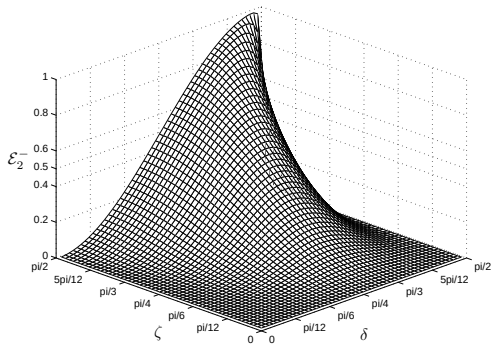

Fig. 15. $\mathcal{E}_2^-$ as function of ζ and δ for $\nu_s = 0.4$.

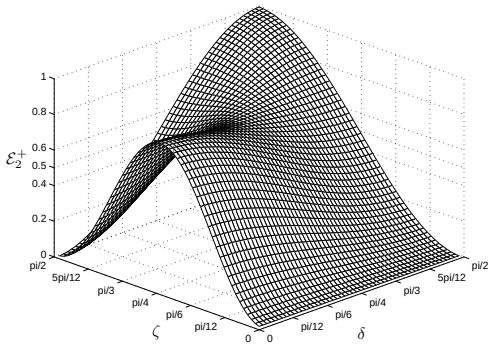

Fig. 16. $\mathcal{E}_2^+$ as function of ζ and δ for $\nu_s = 0.4$.

cores are not used in sandwich panels because they are not resistant enough. When decreasing ζ from $\pi/2$, the prismatic pattern becomes wavy and this waviness increases the faces buckling strength under loading in direction 1.

4. Finite element bounds

The analytical bounds proposed in the previous section are based on the piecewise uniform stress or strain assumption. In order to assess the validity of this assumption, a Finite Element analysis is conducted. The resulting numerical bounds will be compared to the analytical bounds.

4.1 The finite element model

The computation of the transverse shear moduli for both directions and both loading cases (stress and displacement) has been performed within the linear elasticity framework. The unit cell of Fig. 3 is chosen as a representative volume element. Two loadings are applied in each direction: For the upper (respectively, lower)

bound, the prescribed displacements (respectively, forces per unit length) are applied to the AB, BA', DC, CD', $A''B''$, $B''A'''$ edges and the periodicity conditions are applied to the AD, DA'', $A'D'$, $D'A'''$ edges (the strain components at edge AD are set equal to those at edge $A'D'$, for instance).

Since faces are very thin, Kirchhoff shell elements are used. Four elements of the ABAQUS software (triangles P1 (STRI3), triangles P2 (STRI65), quadrangles P1 (S4R5) and quadrangles P2 (S8R5)) were tested and compared through a convergence analysis. Element S4R5 with a 441 node mesh gives accurate results for a low computation cost.

Few detailed chevron folded core geometries are available in accessible literature. Similarly to [3], the following geometric parameters are investigated with $E_s = 3GPa$ and $\nu_s = 0.4$: $a_0 = 30\ mm$, $b_0 \in [20\ mm, 60\ mm]$, $t = 0.1mm$, $\delta = 72°$, $\zeta = 34°$. The analytical normalized bounds for these configurations are:

$$0.23 < \mathcal{E}_1 < 0.71$$
$$0.09 < \mathcal{E}_2 < 0.35$$

Fig. 17 and 18 shows the stresses in the unit cell when submitted to stress loads for the case $a_0 = b_0 = 30mm$. At first sight, it is clear that the stresses are approximately piecewise uniform in each face which is consistent with the assumption made for the analytical derivation of the lower bounds. Also, the stress distribution complies to the symmetries described in section 2. For stress loading in direction 1, the main component is σ_{uu} as predicted with the Warren truss beam analogy. In direction 2, the analytical estimations ($\frac{t\sigma_{uu}}{a_0\tau_2} \approx 0.7$, $\frac{t\sigma_{vv}}{a_0\tau_2} = 0$, $\frac{t\sigma_{uv}}{a_0\tau_2} \approx -0.3$) are in good agreement with FE results.

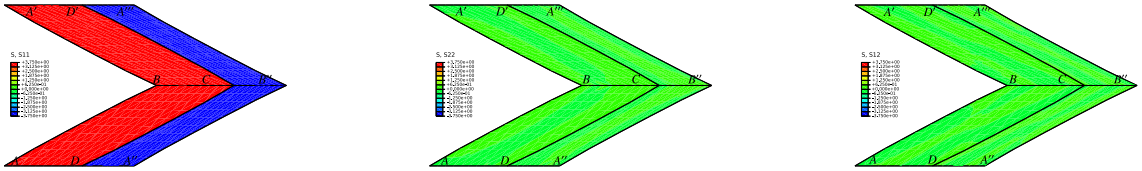

Fig. 17. σ_{uu}, σ_{vv}, σ_{uv} stress components, τ_1 load, $\delta = 72°$, $\zeta = 34°$.

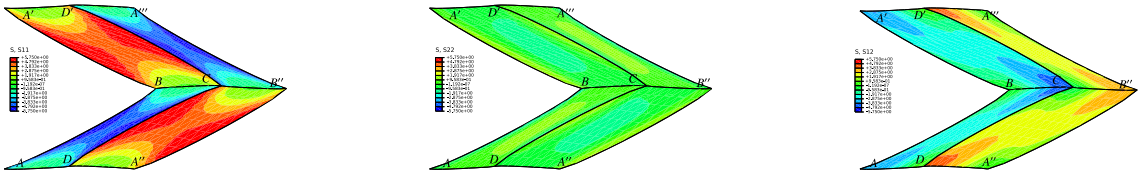

Fig. 18. σ_{uu}, σ_{vv}, σ_{uv} stress components, τ_2 load, $\delta = 72°$, $\zeta = 34°$.

Fig. 19 and 20 show the strains in the unit cell when submitted to strain loads. Again, strains are approximately piecewise uniform in each face. For strain loading in direction 1, analytical estimations are $\frac{\varepsilon_{uu}}{\gamma_1} \approx 0.29$, $\frac{\varepsilon_{vv}}{\gamma_1} \approx 0.20$, $\frac{\varepsilon_{uv}}{\gamma_1} \approx 0.40$. FE fields are approximately consistent with this prediction. In direction 2, analytical estimations are $\frac{\varepsilon_{uu}}{\gamma_2} = 0$, $\frac{\varepsilon_{vv}}{\gamma_2} \approx 0.14$, $\frac{\varepsilon_{uv}}{\gamma_2} \approx 0.53$. The FE fields are quite homogenous in each face and they are closer to the analytical predictions.

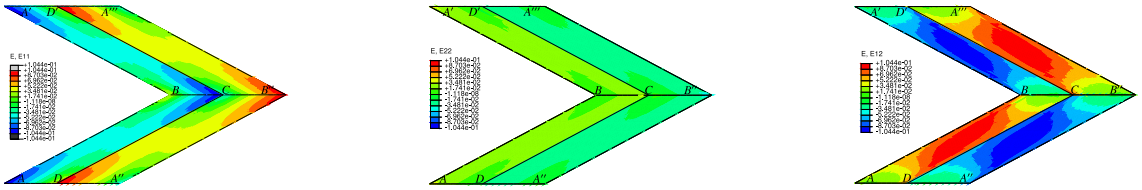

Fig. 19. ε_{uu}, ε_{vv}, ε_{uv} strain components, γ_1 load, $\delta = 72°$, $\zeta = 34°$.

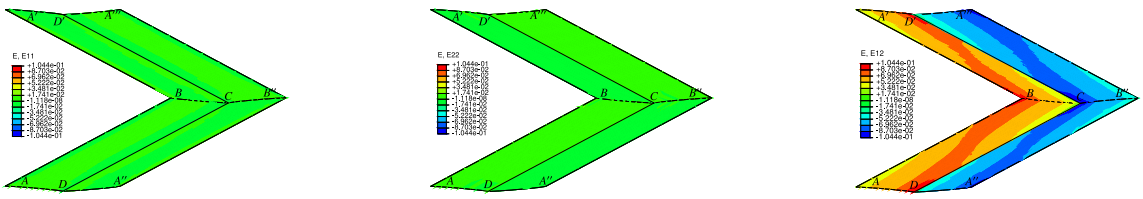

Fig. 20. ε_{uu}, ε_{vv}, ε_{uv} strain components, γ_2 load, $\delta = 72°$, $\zeta = 34°$.

FE analysis has been also performed for several values of the shape ratio a_0/b_0. Results are shown on Fig. 21 and 22.

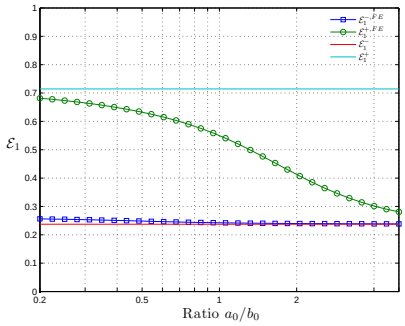

Fig. 21. Bounds in direction 1 versus a_0/b_0 for $\delta = 72°$, $\zeta = 34°$ and $\nu_s = 0.4$.

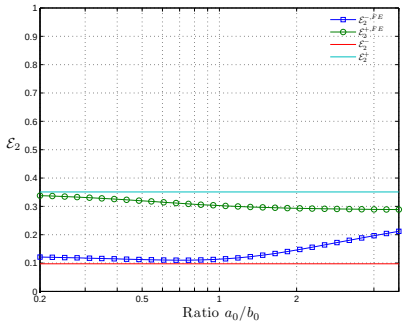

Fig. 22. Bounds in direction 2 versus a_0/b_0 for $\delta = 72°$, $\zeta = 34°$ and $\nu_s = 0.4$.

4.2 Results

For all shape ratios, the expected hierarchy between bounds is observed: $\mathcal{E}_\alpha^- < \mathcal{E}_\alpha^{-,\,FE} < \mathcal{E}_\alpha^{+,\,FE} < \mathcal{E}_\alpha^+$. For direction 1, on the one hand, the FE lower bound is really close to the analytical lower bound whatever the shape ratio is. This good agreement is consistent with the good uniformity of the stresses shown in Fig. 17. On the other hand, the FE upper bound is dependent of the shape ratio. In fact, the computed strain fields are not homogenous in this case (Fig. 19). Moreover, it should be emphasized that the numerical FE bounds for direction 1 cover all the range between the analytical upper and lower bounds as the shape ratio varies. For direction 2, the FE upper bound is not really affected by the shape ratio and the strain fields are quite uniform. The FE lower bound seems more dependent on the shape ratio and the stress fields are less uniform. As expected, when the actual fields are almost piecewise uniform, then the analytical and numerical bounds are consistent.

One important conclusion of this study is that both FE and analytical bounds are loose for practical values of the shape ratio ($a_0/b_0 \in [0.5, 1.5]$). This means that the effective transverse shear moduli of the considered chevron pattern ($\delta = 72°$, $\zeta = 34°$) are sensitive to the the skin effect.

Finally, a systematic computation has been performed for δ and ζ ranging between 0 and $\pi/2$ for $a_0/b_0 = 1$. The obtained figures (23, 24, 25, 26) are similar to those obtained for the analytical bounds.

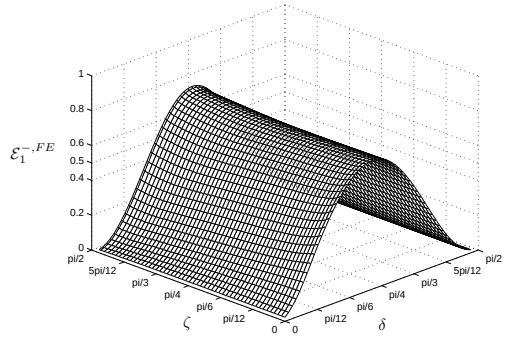

Fig. 23. $\mathcal{E}_1^{-,FE}$ as function of ζ and δ for $\nu_s = 0.4$ and $a_0/b_0 = 1$.

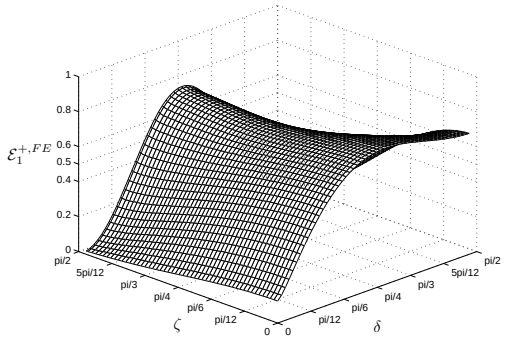

Fig. 24. $\mathcal{E}_1^{+,FE}$ as function of ζ and δ for $\nu_s = 0.4$ and $a_0/b_0 = 1$.

4.3 Comparison with honeycomb

It is of interest to compare honeycomb geometries with Chevron pattern. For a regular honeycomb core with the same wall thickness, the use of piecewise uniform strain and stress in the core walls gives equal lower and upper bounds: $\mathcal{E}_1 = \mathcal{E}_2 = 0.5$. In order to compare chevron pattern to honeycomb, the sum $\Sigma = \mathcal{E}_1 + \mathcal{E}_2$ can be considered. Its upper bound for all honeycomb geometries is $\Sigma^+ = 1$ [13]. However, for chevron pattern, it is:

$$\Sigma^+ = \left(\frac{2}{1-\nu_s}\cos^2\delta\sin^2\zeta + 1\right)\left(1 - \cos^2\delta\sin^2\zeta\right) \qquad \text{(eq. 16)}$$

which reaches the maximum value:

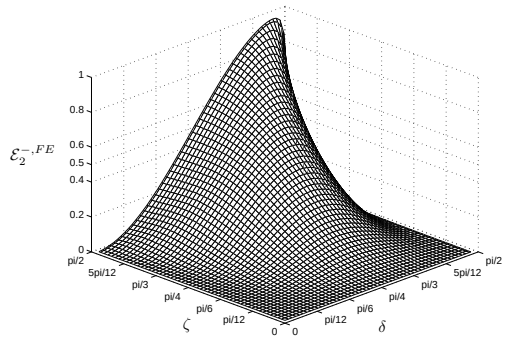

Fig. 25. $\mathcal{E}_2^{-,FE}$ *as function of* ζ *and* δ *for* $\nu_s = 0.4$ *and* $a_0/b_0 = 1$.

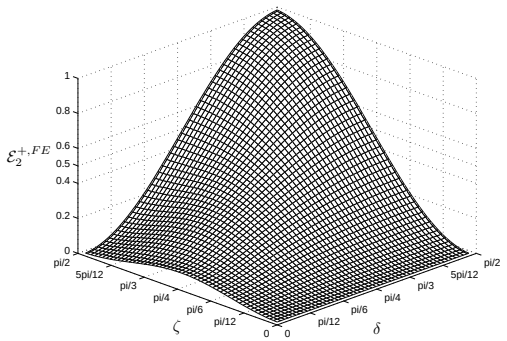

Fig. 26. $\mathcal{E}_2^{+,FE}$ *as function of* ζ *and* δ *for* $\nu_s = 0.4$ *and* $a_0/b_0 = 1$.

$$\frac{(3-\nu_s)^2}{8(1-\nu_s)} \qquad \text{for} \qquad \cos^2\delta \sin^2\zeta = \frac{1+\nu_s}{4} \qquad \text{(eq. 17)}$$

Fig. 27 shows Σ^+ as function of ζ and δ for $\nu_s = 0.4$, and the continuous set of (ζ, δ) couples for which Σ^+ reaches its maximum value. Thus, considering Σ^+, the chevron pattern can potentially outperform honeycomb stiffness by $\simeq 40\%$ for usual values of ν_s. In Fig. 28 the FE computed sum of upper bounds $\Sigma^{+,FE}$ is plotted

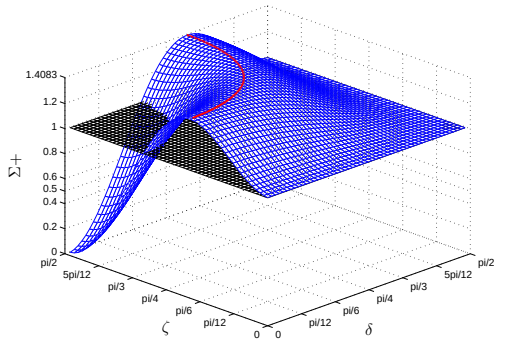

Fig. 27. $\Sigma^+ = \mathcal{E}_1^+ + \mathcal{E}_2^+$ *as function of* ζ *and* δ *for* $\nu_s = 0.4$.

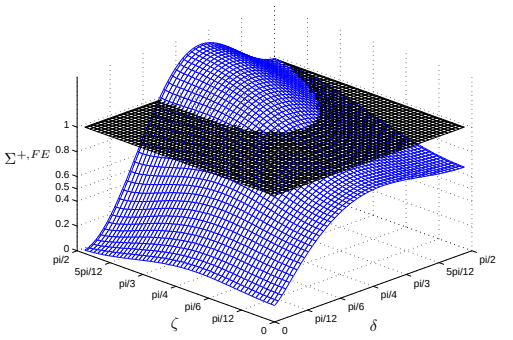

Fig. 28. $\Sigma^{+,FE} = \mathcal{E}_1^{+,FE} + \mathcal{E}_2^{+,FE}$ *as function of* ζ *and* δ *for* $\nu_s = 0.4$ *and* $a_0/b_0 = 1$.

for a shape ratio $a_0/b_0 = 1$. As expected FE upper bounds are lower than analytical upper bounds. The domain where Chevron pattern outperforms honeycomb geometries ($\Sigma^{+,FE} > 1$) is smaller but still includes geometries that can be machined. For the geometry considered in [3], $\Sigma^{+,FE} \simeq 0.65$.

5. Conclusion

For an out-of-plane loaded sandwich panel with stiff skins (0.6 mm of CFRP for instance), usual chevron folded core thickness (0.1 mm of impregnated aramid paper) and small slenderness ratio (1/10 for example), the deflection is almost proportional to the effective transverse shear moduli of the chevron folded core. In this paper, Kelsey *et al.*'s method has been applied for the derivation of analytical and numerical upper bounds for these moduli. For some pattern geometries, the exact values have been founded. Moreover, it has been shown that for some geometries, the chevron folded cores are stiffer than honeycomb-like cores (lower bounds for chevron core are higher than upper bounds for honeycombs). Finally, this work sets the path for the derivation of analytical bounds for other folded core geometries such as M-type core [19].

However, the obtained bounds for the already existing pattern geometries [3], $\delta = 72°$, $\zeta = 34°$, are too loose (more than 100% of discrepancy). This difficulty was already pointed out in [1] for honeycomb-like cores. It is due to the lack of consideration of the interaction between the skins and the core of the sandwich panel. According to these authors, the upper bound is relevant for sandwich panels with thick skins while the lower bound is relevant for thin skins.

In the case of honeycomb-like core, the discrepancy between bounds has been identified as a skin effect (Chen and Davalos [16], Xu and Qiao [20]) and correlated to the ratio between the cell width and the core thickness. In the case of Chevron folded core, the great discrepancy between the obtained bounds necessitates more refined models able to take into account the interaction between the skins and the core.

Thus, it seems necessary to consider more elaborated homogenization method [14, 20, 16, 21] or the Reissner-Mindlin homogenization method proposed by Sab and his co-workers [22, 23, 15, 24, 25].

Références

[1] S. Kelsey, R.A. Gellatly, and B.W. Clark. «The shear modulus of foil honeycomb cores: A theoretical and experimental investigation on cores used in sandwich construction». *Aircraft Engineering and Aerospace Technology*, 30(10):294 – 302, 1958.

[2] B. Basily and E.A. Elsayed. «Dynamic axial crushing of multi-layer core structures of folded chevron patterns». *International Journal of Materials and Product Technology*, 21:169–185, 2004.

[3] M.Q. Nguyen, S.S. Jacombs, R.S. Thomson, D. Hachenberg, and M.L. Scott. «Simulation of impact on sandwich structures». *Composite Structures*, 67(2):217–227, February 2005.

[4] S. Heimbs, T. Mehrens, P. Middendorf, A. Maier, and M. Schumacher. «Numerical determination of the nonlinear effective mechanical properties of folded core structures for aircraft sandwich panels». 6^{th} European LS DYNA User's Conference, 2006.

[5] M. Kintscher, L. Karger, A. Wetzel, and D. Hartung. «Stiffness and failure behaviour of folded sandwich cores under combined transverse shear and compression». *Composites Part A: Applied Science and Manufacturing*, 38(5):1288–1295, May 2007.

[6] D. H. Kling. *Paterning technology for folded sheet structures*. US Patent: US 6,935, 997 B2, (30/08/2005).

[7] B. Basily and A. Elsayed. *Technology for continuous folding of sheet materials*. US Patent: US 7, 115, 089 B2, (03/10/2006).

[8] B. Basily and A. Elsayed. «A continuous folding process for sheet materials». *International Journal of Materials and Product Technology*, 21:217–238, 2004.

[9] R. Kehrle and Deutschland Airbus. *Method for the production of a sandwich structure for a sandwich composite*. World Patent: WO 2004/043685 A2, (27/05/2004).

[10] S. Heimbs. «Virtual testing of sandwich core structures using dynamic finite element simulations». *Computational Materials Science*, 45(2):205 – 216, 2009.

[11] L. J. Gibson and M. F. Ashby. *Cellular solids*. Pergamon Press, 1988.

[12] J. Hohe and W. Becker. «Effective stress-strain relations for two-dimensional cellular sandwich cores: Homogenization, material models, and properties». *Applied Mechanics Reviews*, 55(1):61–87, 2002.

[13] X. Frank Xu, Pizhong Qiao, and J. F. Davalos. «Transverse shear stiffness of composite honeycomb core with general configuration». *Journal of Engineering Mechanics*, 127(11):1144–1151, 2001.

[14] J. Hohe. «A direct homogenisation approach for determination of the stiffness matrix for microheterogeneous plates with application to sandwich panels». *Composites Part B: Engineering*, 34(7):615–626, October 2003.

[15] A. Cecchi and K. Sab. «A homogenized reissner-mindlin model for orthotropic periodic plates: Application to brickwork panels». *International Journal of Solids and Structures*, 44(18-19):6055–6079, September 2007.

[16] A. Chen and J. F. Davalos. «A solution including skin effect for stiffness and stress field of sandwich honeycomb core». *International Journal of Solids and Structures*, 42(9-10):2711 – 2739, 2005.

[17] I.M. Zakirov, K.A. Alekseev, and G.V. Movchan. «Influence of coating thickness on geometric parameters of a chevron core». *Russian Aeronautics*, 51(3):326 – 329, 2008.

[18] E. Reissner. «Reflections on the theory of elastic plates». *Applied Mechanics Reviews*, 38(11):1453 – 1464, 1985.

[19] S. Heimbs, P. Middendorf, S. Kilchert, A. Johnson, and M. Maier. «Experimental and numerical analysis of composite folded sandwich core structures under compression». *Applied Composite Materials*, 14(5):363–377, November 2007.

[20] X. Frank Xu and Pizhong Qiao. «Homogenized elastic properties of honeycomb sandwich with skin effect». *International Journal of Solids and Structures*, 39(8):2153 – 2188, 2002.

[21] D. H. Pahr and F. G. Rammerstorfer. «Buckling of honeycomb sandwiches: Periodic finite element considerations». *Cmes-Computer Modeling In Engineering & Sciences*, 12(3):229–241, April 2006.

[22] A. Cecchi and K. Sab. «A comparison between a 3d discrete model and two homogenised plate models for periodic elastic brickwork». *International Journal of Solids and Structures*, 41(9-10):2259–2276, May 2004.

[23] V. T. Nguyen, J. F. Caron, and Karam Sab. «A model for thick laminates and sandwich plates». *Composites Science and Technology*, 65(3-4):475 – 489, 2005. JNC13-AMAC-Strasbourg.

[24] T. K. Nguyen, K. Sab, and G. Bonnet. «Shear correction factors for functionally graded plates». *Mechanics of Advanced Materials and Structures*, 14(8):567–575, 2007.

[25] T. K. Nguyen, K. Sab, and G. Bonnet. «First-order shear deformation plate models for functionally graded materials». *Composite Structures*, 83(1):25–36, March 2008.